Archives of Civil and Mechanical Engineering (2023) 23:125
https://doi.org/10.1007/s43452-023-00673-z

ORIGINAL ARTICLE

Effect of number of tool shoulders on the quality of steel to magnesium alloy dissimilar friction stir welds

Hassanein I. Khalaf[1] · Raheem Al-Sabur[1] · Hamed Aghajani Derazkola[2]

Received: 18 January 2023 / Revised: 6 April 2023 / Accepted: 12 April 2023

Abstract
Due to magnesium and iron's immiscibility, joining magnesium alloy and steel with modern welding procedures like friction stir welding (FSW) is still complicated. Insufficient chemical bonding and mixing of raw materials in the stir zone are the main problems of joining magnesium alloy and steel. Accordingly, this paper aims to use tools with different numbers of shoulders to boost the properties of the final joint. The different tools with 1, 2, 3 and 4 shoulders were produced and used between magnesium alloy and steel during FSW. The thermal changes during the process are monitored, material flow and mechanical properties are investigated, and fractography is done on the tensile test samples. The results show that increasing shoulder numbers enhances frictional heat generation but not leads to more mechanical interlocking of base metals at interfaces. The maximum heat was generated when welded by two shoulders (600 °C), and the lowest heat was generated in one shoulder joints (540 °C). The number of shoulders for achieving the best mechanical properties has limitations. The results show that the final quality of the joint improves from one shoulder tool to three, but shows decreases at joints that were welded by more than three shoulders. The most robust tensile strength was recorded in two shoulder samples (210 MPa) with brittle fracture behavior.

Keywords Friction stir welding · Steel · Magnesium · Tool shoulder · Pin profile

1 Introduction

Lightweight alloys are widely used in various applications due to their high strength-to-weight ratio, which helps in reducing fuel consumption. The fuel consumption is reduced by up to 7% for each 10% weight reduction. These alloys find applications in the aerospace, automotive, and construction industries [1]. In aerospace, lightweight alloys reduce aircraft weight, leading to lower fuel consumption and emissions. In the automotive industry, lightweight alloys make vehicles more fuel-efficient [2]. Using steel, aluminium, and magnesium alloys effectively achieves economic, safe, and lightweight structures [3]. Depending on the fact that magnesium alloys are one of the lightest structural materials with outstanding mechanical properties, their applications have recently increased dramatically, especially in vehicles. On the other hand, the properties of steel, such as high toughness, good strength, and reasonable price, make it difficult to replace. Replacing full steel joints with steel–Mg joints can help achieve an optimum strength-to-weight ratio of automobile structures. Various ways exist to join dissimilar metals, including adhesives [4], and hybrid riveting [5], for combining mechanical fastening and adhesion benefits. The large difference in the melting point between iron and magnesium, which reaches about three times, is the biggest obstacle to their welding processes, especially in fusion welding [6]. Over the past two decades, FSW, a type of solid-state welding, has been developed [7]. In the FSW process, the base metal softens by employing friction heat and stirring using a rotating cylindrical tool with a pin at its ends. The pin is fully inserted into the sheets while the shoulder surface contacts the upper sheet surface to produce the required frictional heat [8]. The FSW fields were rapidly expanded and developed, and their applications covered many industries, especially aerospace and batteries. It is no longer limited to joining metals but is now widely used in dissimilar alloys of

✉ Hamed Aghajani Derazkola
h.aghajani@deusto.es

[1] Mechanical Department, Engineering College, University of Basrah, Basrah 6100, Iraq

[2] Department of Mechanics, Design and Industrial Management, University of Deusto, Avda Universidades 24, 48007 Bilbao, Spain

Published online: 24 April 2023

the same metals [9] or dissimilar metals applications [10]. Moreover, FSW is now used in non-traditional and promising techniques, such as underwater welding for low-carbon steel [11] and for aluminium alloys [12] and joining polymers [13] or joining them to metals [14]. Several studies have shown that FSW is a promising method for welding magnesium with various steel alloys. Magnesium alloy AZ31 (3% Al, 1%Zn) is the most widely used in FSW studies for joining Mg with several types of steel alloys. Abe et al. [15] use butt joint FSW to join a mild steel plate and a magnesium alloy plate in a butt configuration. The results demonstrated a successful joint, achieving a maximum strength of 70% of the magnesium base metal. The study also found that the pin rotation speed and offset impacted the joint strength and microstructure. The same joint configuration of the previous study was studied by Watanabe et al. [16], revealing that joint strength was 70% of the magnesium base metal. Low rotation speed caused defects in Mg, while high rotation speed caused magnesium ignition, reducing joint strength. Careful consideration of pin rotation speed is necessary to maintain joint integrity. Jana et al. [17] examined the joining of AZ31 Mg alloy to mild steel and HSLA using the FSW process. Intermetallic phases were not observed in both cases, so they considered the joint mainly emanating strength from the mechanical hooks. Furthermore, an Mg–Zn layer was formed during the process due to reacting the melted Zn with Mg. According to Schneider et al. [18], the inadequate metallic bond formation between steel and magnesium in FSW was caused by the difficulty of flowability due to the many fragmented steel particles present near the joint interface. Moreover, they confirmed that the fracture strength of the joint is significantly improved when zinc coating is added to the steel, especially when the welding speed is high. Furthermore, Jana et al. [19] investigated the effectiveness of friction stir welded joints under dynamic loads when joining AZ31 magnesium alloy to Zn-coated mild steel and high-strength low-alloy steel (HSLA). They noticed a crack initiation in the interface region between the AZ31 and HSLA, and the major failure mode occurred at the top of the AZ31 sheet. Several studies attempted to provide a clearer picture of the joining of AZ31 magnesium alloy to Zn-coated steel using FSW. The effect of tool geometry on joint microstructure and mechanical properties was investigated. In lap configuration FSW, researchers analyzed the microstructures and mechanical properties of the joints. The presence of the zinc coating promoted the formation of an Mg–Zn low-melting-point eutectic structure at the interface. The welding speed was found to significantly affect the failure loads of the joints at a rotation speed of 1500 rpm [6]. In addition, the choice of pin length affected the quality and strength of lap joints between zinc-coated and brushed-finish steel. Short pins were optimal for zinc-coated steel, while long pins improved failure loads for brushed-finish steel. Failure patterns differed between the two, with long-probe joints fracturing at the magnesium alloy side and short-probe joints fracturing at the joining interface [20]. Zhang et al. [21] confirmed that the stacking sequence significantly impacts joint strength when the keyhole-less lap friction stir spot welding process joins AZ31B to mild steel. They also noticed that the stacking sequence leads to an unstable and narrow process window, forming intermetallic compounds at the interface region. Wei et al. [22] noticed that the flashes, zippers, and scraps during the FSW of the SUS302 stainless steel to the AZ31 magnesium alloy led to the production of interfacial morphologies, which are responsible for the metallurgical bonding during the process. They also indicated that the shear strength values did not affect by the joint configuration, either lap or butt. Uematsu et al. [23] used pin-less friction stir spot welding to join Mg/steel alloys and compare them with Al/steel ones. In the welding nugget, they reported that the material flow and the exhibited static tensile in the magnesium/steel were less than the aluminium/steel. On the other hand, the possibility of bonding dual-phase steel (DP steel) with magnesium alloys has been studied more extensively than other alloy steels. Kulkarni et al. [24] provided a modelling approach with experimental validation for joining uncoated DP590 steel with AZ31 alloy using the Friction Stir-Assisted Scribe process. Later, Das et al. [25] used the same process as before to compare joining DP590 steel with AZ31 and pure magnesium to study the interface characterization. Suryakanta et al. [26] and Banglong et al. [27] joined DP600 to AZ31 alloy, where the effect of weld parameters on joint quality during FSW studies in the first study and refill friction stir spot welding (RFSSW) in the second one was investigated. RFSSW uses a specially designed filler material to fill the hole created by the rotating tool, which formally appeared in the FSW processes. In addition, the RFSSW was used to join DP600 with ZEK100 magnesium alloy to examine the microstructures [28] and fatigue behaviour [29]. Finally, the dual-phase steel DP600 was joined with AM60 magnesium alloy to examine the joint formation [30]. The surface profile of the shoulder peripheral is important for FSW joint performance. The shoulder profile of cylindrical, conical, flat, concave, and convex is widely used [31]. Furthermore, the shoulder end surface features are essential for good performance. FSW processes also extensively use featureless, concentric circles, ridged, scrolled, grooved, and knurled shapes [32]. Most studies did not consider the shoulder's shape at FSW joints.

In summary, FSW is a reliable welding method for joining magnesium alloys and steel because it produces sufficient chemical bonding and reduces welding defects. However, a new FSW tool could further enhance the process by improving material mixing and temperature distribution and addressing specific challenges when welding these materials. The new tool would lead to stronger, more reliable

Table 1 Chemical composition of base metals

Element (wt%)	Al	Mn	Si	Zn	Mg	C	S	Fe
AZ31	2.5–3.5	0.2	0.1	0.6–1.4	96	–	–	–
AISI 1006	–	0.24–4	–	–	–	0.08	0.05	99.5

Table 2 Mechanical property of base metals

Mechanical property	AZ31 magnesium	AISI 1006 steel
Density (kg/m^3)	1800	7800
Tensile strength (MPa)	268	330
Yield strength (MPa)	200	285
Shear strength (MPa)	140	230
Elongation at break (%)	15	32
Hardness (Brinell)	49	95
Melting point (°C)	630	1470
Specific heat at 25 °C (J/g-°G)	1.00	0.481
Thermal conductivity at 25 °C (W/m-K)	96	53

joints with better properties, making the FSW process even more effective for joining magnesium alloys and steel. This study developed a new tool design with several shoulders to investigate the maximum tensile shear stress and the maximum generated temperature. The study will be supported with experimental tests with scanning electron microscopy (SEM) and energy dispersive X-ray spectrometry (EDS) to investigate the thermal analysis, chemical interaction, and surface and internal flows.

2 Experimental procedure

2.1 Base metals

This research selected AZ31 magnesium alloy and low-carbon steel (AISI 1006) as raw materials. The chemical composition of raw materials are presented in Table 1. AZ31 and AISI 1006 steel samples were cut from 3 mm thick sheets. The mechanical properties of raw materials tested in the laboratory and the mean value of mechanical properties are reported in Table 2. Before the FSW procedure, the edges of the base materials were cleaned and deoxidized.

2.2 Welding tool

Four different tools were designed to study the effects of tool shoulders during the process. All tools had an 18 mm diameter and 2.6 mm pin length, and each of them had a different number of shoulders. Each tool had a different name—all were made of tungsten carbide. The tools' size, geometry and name are presented in Fig. 1. The FSW tool with 1, 2, 3 and 4 shoulders is named Tool I, Tool II, Tool III and Tool IV, respectively.

2.3 Welding procedure

For the welding procedure, a milling machine was modified to do the FSW process (as an FSW machine). The FSW process has been done at ambient temperature. A steel-made fixture is set on the FSW machine to fix raw materials during welding. The raw materials are fixed with butt joint configuration. During the FSW process, all tools had the same parameter. The tools travelling speed, rotational velocity, tilt angle and plunge depth were 60 mm/min, 790 rpm, 1° and 0.2 mm, respectively. The welding tool had not offset, and parameters were selected after pre-tests and are optimum process parameters. Two K-type (Omega) thermocouples are placed on the magnesium and steel sides to record the temperature.

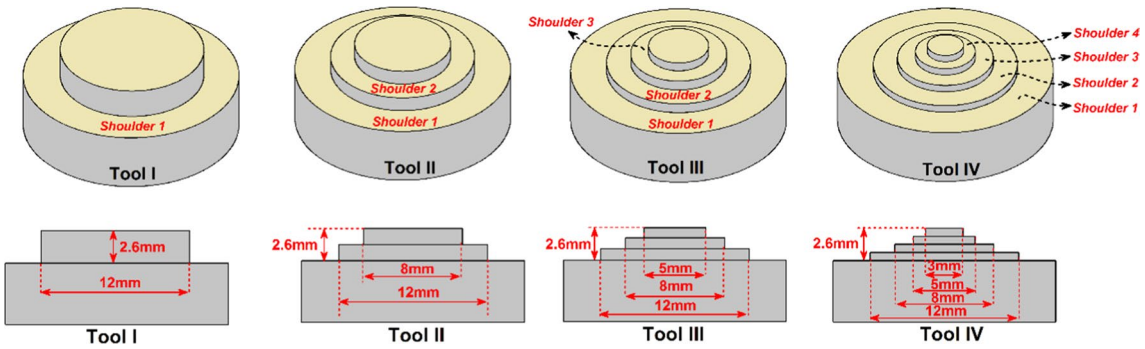

Fig. 1 FSW tools with I, II, III and IV shoulders

The thermocouples were placed 9.5 mm from the raw materials interface. A picture of the welding procedure is presented in Fig. 2a.

2.4 Sample characterization

After the FSW process, the welded samples' surface flow, internal flow, tensile strength test and hardness evaluation were done. SEM investigated the internal material flow. The tensile test of samples was carried out according to ASTM E08 standard number. Three tensile tests have been done, and average values are reported in this study after tensile test fractography analysis from the fracture surface of the tensile sample carried out with SEM. A Brinell hardness test has been done on welded samples according to the ASTM E10 standard with1 mm indentor, 300N load 30 degree of loading.

3 Results and discussions

3.1 Thermal study

The generated heat during FSW consists of frictional heat and plastic deformation. The pin profile can affect the friction coefficient and applied normal force at the interface of base metals, leading to a change in frictional heat generation during FSW. As mentioned in the experimental section, thermocouples recorded the temperature of the joint line during the FSW process. A schematic view of thermocouple placement is presented in Fig. 3a. As a sample. The recorded frictional heat at the joint welded by Tool II is presented in Fig. 3b. Dissimilar material caused the recorded heat in the advancing and retreating sides to differ. The results show that the recorded temperature on the steel side was more than magnesium side. The higher shear strength of steel compared to magnesium alloy leads to more heat production by the FSW tool. Comparing the recorded maximum heat in various samples is presented in Fig. 3c.

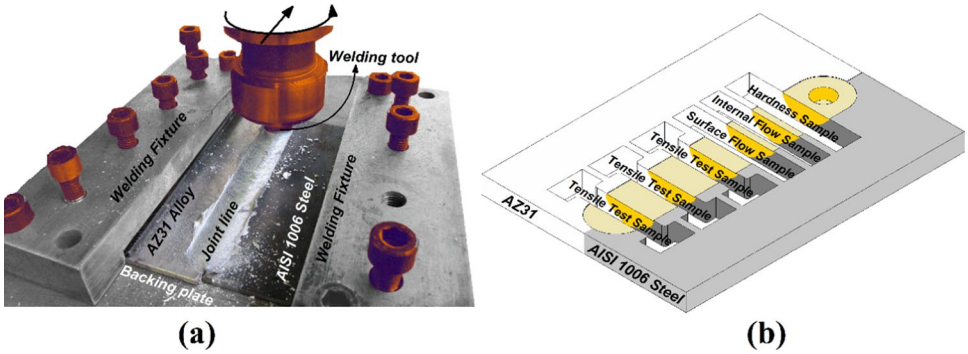

Fig. 2 **a** FSW fixture and a sample of welding procedure, **b** schematic view of mechanical test sampling

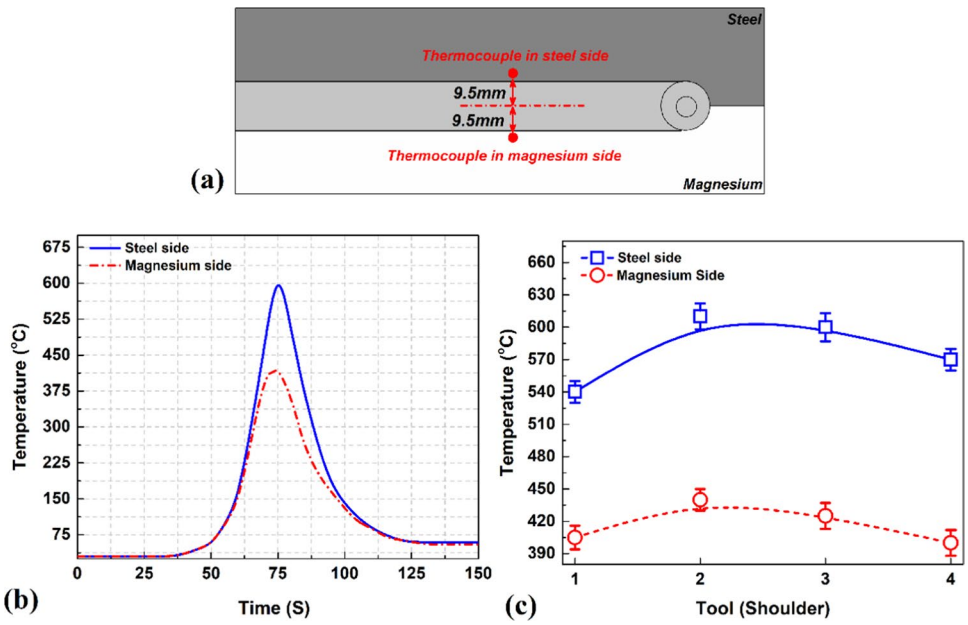

Fig. 3 **a** Schematic view of thermocouple placement. **b** Recorded temperature by Tool II, **c** comparisons between the maximum temperature at steel and magnesium sides by different tools

Due to obtained results, the minimum temperature was recorded by Tool IV and the maximum temperature was recorded by Tool II. The recorded temperature had increased from Tool I to Tool II and then decreased. The increasing number of tool shoulders by more than two decreases tool efficacy from a generation heat point of view. From a geometrical point of view, more than two shoulder tool acts like a frustum pin profile. The difference in recorded heat between Tool II and Tool III is not huge, but the maximum heat dropped sharply after that. The maximum temperature on the steel side recorded at joint Tools I, II, III, and IV was 540, 603, 582, and 565 °C, respectively. The maximum temperatures on the magnesium side were 400, 426, 419, and 401 °C for Tool I, II, III, and IV. This maximum temperature difference relates to the total contact area of tools with workpieces. A schematic view of the area of tools that are in contact with workpieces is presented in Fig. 4a. The geometry and area of different tools are compared, and the results are presented in Fig. 4b. The geometrical measurement of tools indicates that the total area of Tools I, II, III, and IV are 360, 385, 355 and 350 mm^2. It means the contact area between Tool II and raw materials is maximum, and Tool IV is minimum. The results indicate that the shoulder area increases from Tool I to Tool IV, but the pin side area decreases. The minimum shoulder area is for Tool I (~ 140 mm^2), and the maximum belongs to Tool IV (~ 240 mm^2).

3.2 Surface flow

The surface flow of the joint welded using tools I, II, and IV are presented in Fig. 5a–c, respectively. The surface flow from the visual inspection was similar for all joints. On the other hand, no void defect or the flash is seen on the joint's surfaces. The results revealed small surface cracks on the surface of Tool IV. The cracks were formed near the base metal's interfaces. During the FSW process, all tools' top shoulder diameter (A1 area) was constant. It seems the reason for the formation of surface cracks is related to the pin shapes. The results indicated that generated heat in IV was lower than in Tools II and III and more than in Tool I. It can be concluded that generation heat is not the only factor for mixing raw materials. The stirring action of the pin can affect the internal and surface flow. Due to the results, the stirring action of Tool IV was low and led to surface cracks on the joint line.

The surface flow ring forms due to the plastic deformation of the weldments around the FSW tool during the forward movement. The surface flow ring pattern is formed due to the tool's rotation and transverse direction. The surface flow ring expression indicates the quality of the joint line. A well-formed surface flow ring can indicate that the material has been adequately plasticized and that the weld joint is solid and defect-free. A surface flow ring is a qualitative feature for the joint line with a circular or semi-circular pattern. The weldment that flows around the tool is subjected to severe shear and compression stresses, which causes it to deform and flow in a characteristic pattern. The distance between the formed ring can indicates the quality of plasticized material compression (joint line density) backside of the tool. The tool's total heat generation and stirring action can affect the surface flow and flow rings. The flow ring of joints that FSWed by Tool I, II, and IV are measured and presented in Fig. 5. The statistics results of all samples are presented in the manuscript. As discussed earlier, the results of Tool III are not notable and do not significantly impact the described trend. For this reason, Figures of Tool III ignored and focus on the valuable data that present meaningful information about the number of tool shoulder trends. Due to obtained results, the flow ring distance of Tools I, II, III, and IV were 1.9, 1.6, 1.6, and 2.3 µm, respectively. The tool's heat generation and stirring action change the flow ring distance. Due to obtained results, the lowest distance formed in Tool II and III joints shows that the tool's material compression during joining was more than in other cases. On the other

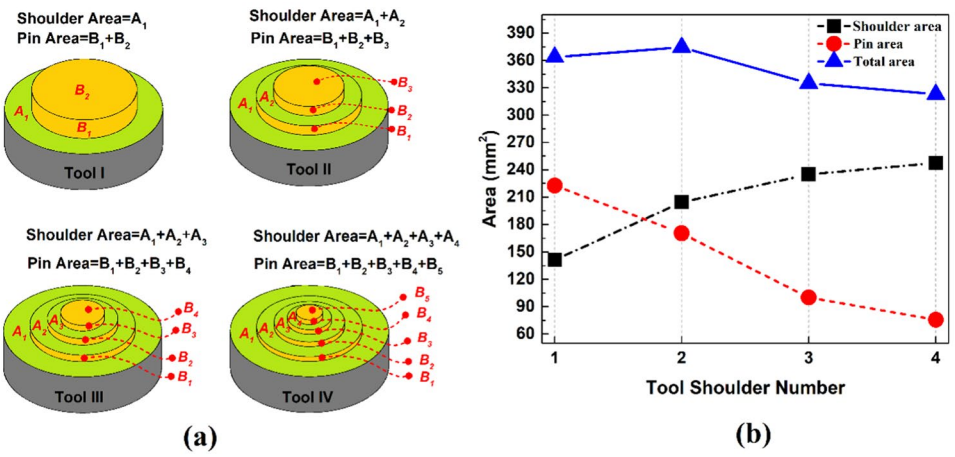

Fig. 4 **a** Schematic view of tool areas, **b** comparisons between contact areas of different tools

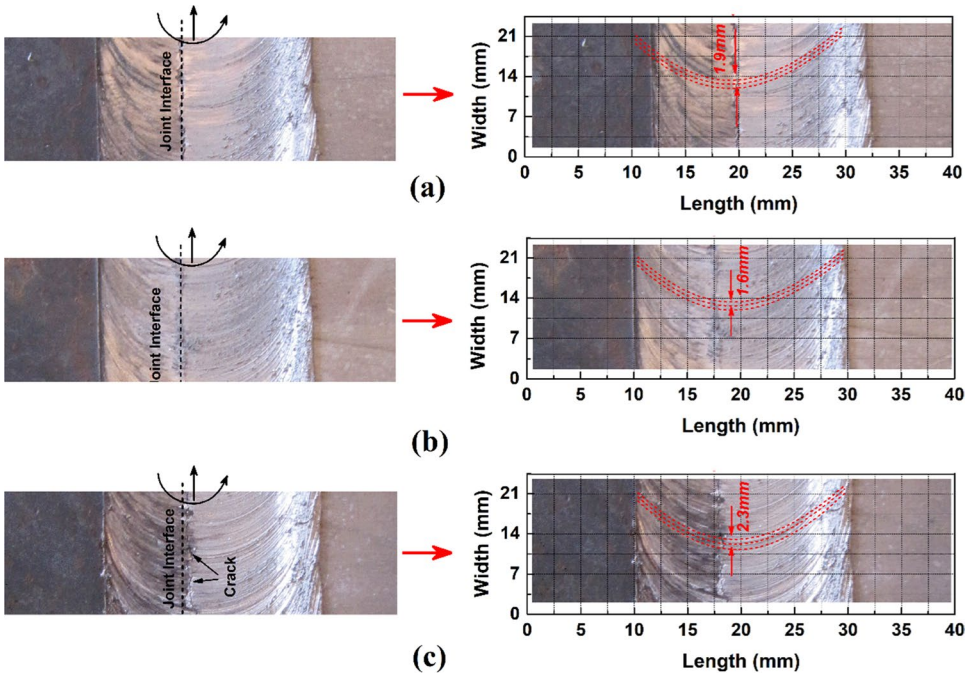

Fig. 5 The surface flow of joints welded by **a** Tool I, **b** Tool II, and **c** Tool IV

hand, a bigger ring flow distance indicates that the mixing of magnesium alloy and steel was not good enough in Tool IV comparing other cases.

The image of the surface microtopography of welded sample is shown in Fig. 6. The surface of joints welded using the tool I, II, and IV are analyzed with 20× magnifications, and the results are presented in Fig. 6a–c, respectively. The results show microscale surface defects formed in all samples, but the defects in Tool II are much less than in other cases. Due to obtained results, the Tool II joint's flow ring distance is shorter than other cases that approve this joint line forms denser than others. Even though these results are on a microscale, but can give valuable output about minor defects on the surface.

3.3 Internal flow

The cross-section from the internal flow of dissimilar joints between magnesium and steel is presented in Fig. 7. The steel is on the left side, and the magnesium is on the right side. The internal flow of joints welded using tools I, II, and IV are presented in Fig. 7a–c, respectively. the joint line shows the two-separate regions. The interaction between magnesium and steel was not intense at the interface. Because no intermetallic layer or lamellar structure formed in the cross-section view, the results show that a stirred zone (SZ) formed at the middle of the joint, and a thermo-mechanical affected zone (TMAZ) and heat affected zone (HAZ) formed on both sides. The basis of

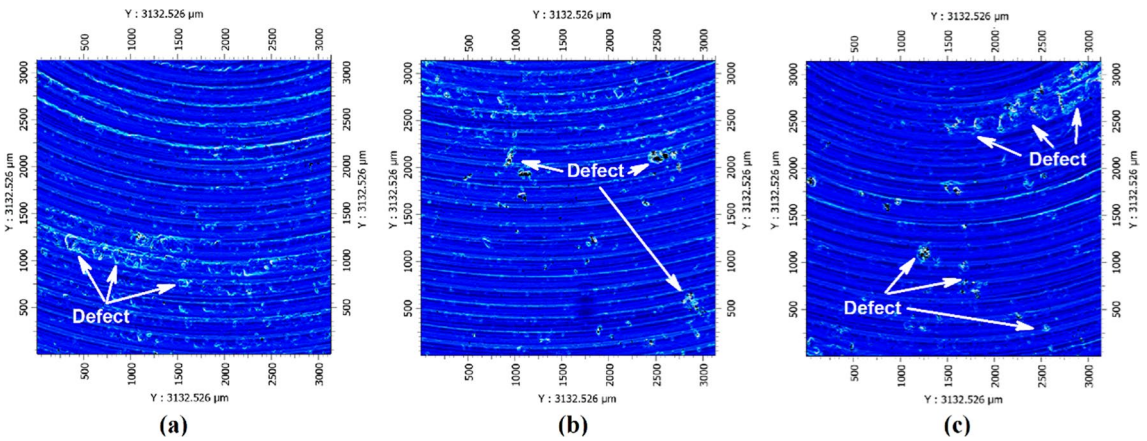

Fig. 6 Surface micro topography of joints that welded by **a** Tool I, **b** Tool II, and **c** Tool IV

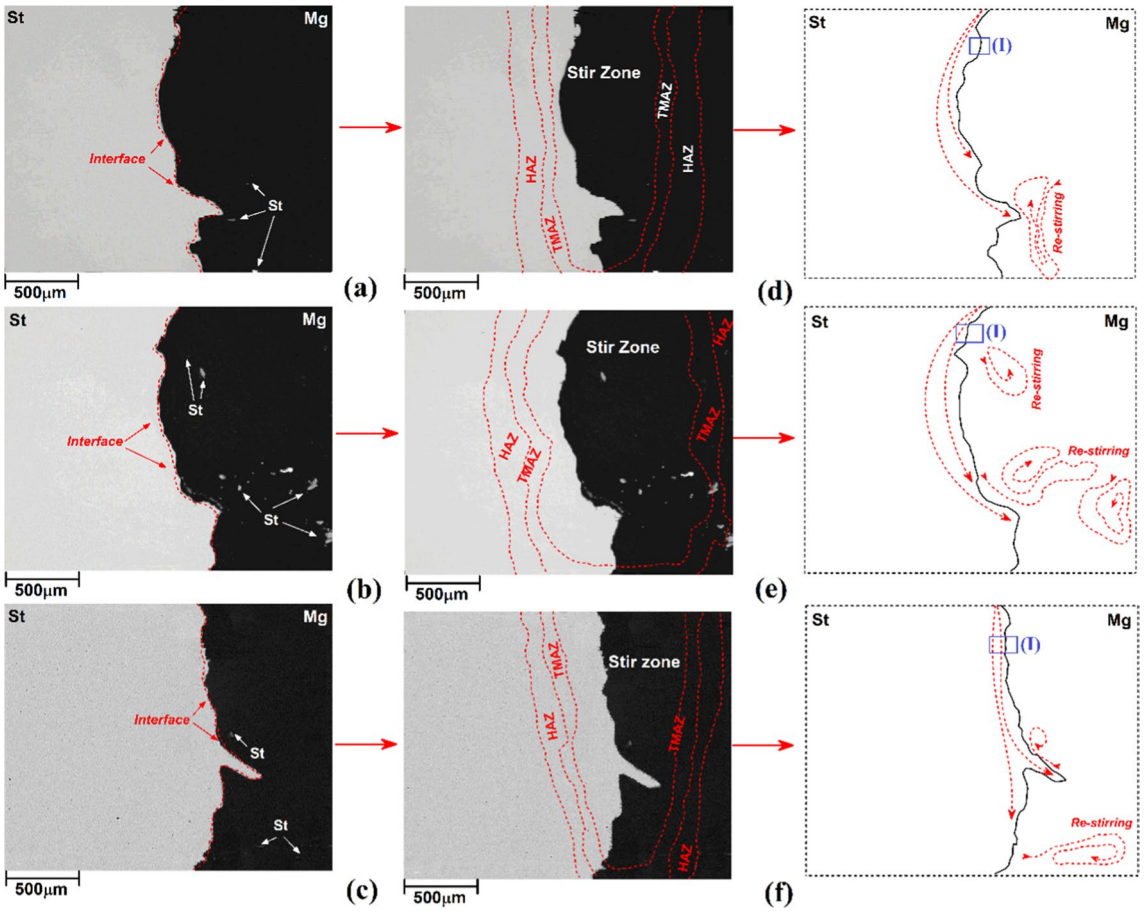

Fig. 7 SEM image from a cross-section of joints welded by **a** Tool I, **b** Tool II, and **c** Tool IV. Schematic view from the internal flow of joints welded by **d** Tool I, **e** Tool II, and **f** Tool IV

finding the SZ, TMAZ, and HAZ area was according to internal flow changes that high magnification investigation by SEM can detect. The SZ consists of the interface of base metals with a small area on the steel side that is deformed by the tool, and a part of magnesium consists of a severe flow pattern and small particles of steel. The TMAZ was a narrow area near SZ with intense flow rings. HAZ was detected in SEM investigation by a thick bond between TMAZ and base metals without deformation. The classification of the different areas was according to the investigation of internal flow during the evaluation of welded samples by SEM. This trend was detected in all samples. The size of SZ increases by increasing the heat generation and the TMAZ and HAZ area. Due to obtained results, the biggest SZ formed in the Tool II joint, and the smallest formed in the Tool IV joint. The HAZ and TMAZ were formed in the Tool II joint with the maximum size and on Tool IV with minimum dimension. In the joint welded using the tool I, the steel stretched into magnesium, and some small steel particles can be detected in the lower area of the stir zone. The schematic view of the internal flow of Tool I, II, and IV joints is presented in Fig. 7d–f, respectively.

As the schematic view depicted, the steel stretched in the bottom side of the pin in one shoulder case. Re-stirring action locally happened in front of stretched steel. In re-stirring area consists of small particles of steel. The re-stirring mechanism in friction stir welding (FSW) using multi-shoulders involves using other shoulders on the rotating tool to re-stir the material behind it as it moves through the joint. In the standard FSW process, the rotating tool creates a stationary stir zone, which remains at the rear of the tool as it moves forward. This can result in incomplete mixing of the material and a lack of bonding between the two materials being joined. The addition of multiple shoulders on the tool allows for the material behind the tool to be re-stirred as it moves forward, resulting in more uniform mixing of the material and improved bonding between the two materials being joined. The re-stirring mechanism also helps to break up any oxide layers or surface contamination, resulting in a higher quality and more reliable joint. In the Tool II sample, steel stretching in magnesium alloy and re-stirring area

increases. Double shoulder increased the interaction between the base material and made a wavy interface between base metals. This wavy interface increases the mechanical interlocking between base metals at the interface. The re-stirring was formed in two areas, one near to second shoulder area and another near beneath the pin. The size of steel particles increases in the Tool II case. With increasing tool shoulder, tool geometry became similar to the frustum pin, and the stirring action of the tool decreased. Even though surface cracks were detected on the surface of the Tool IV joint, the internal flow has no defects or voids. The interface was smooth, and the re-stirring action with steel particles was less than in other cases. The wavy form of the interface In TOOL IV may be seen a little more than in other cases in macro scale (at welding window), but the small waves at interface of Tool IV is much lower than in other Tools.

3.4 Chemical interaction

The EDS analysis of the elements map at the interface of tool II is presented in Fig. 8a. The thin mixture structure with steel particles formed on the magnesium side can be seen. The results show no significant intermetallic components (IMC) formed at the interface.

The image processing from welded samples (Fig. 8b) shows that the size of the particles was not the same. The average number and diameter of steel particle sizes for various samples are presented in Fig. 8c, d, respectively. The results show that the number of steel particles in the magnesium side of joints welded using tools I, II, II, and IV was 100, 120, 105, and 84, respectively. Due to obtained results stirring action of pins leads to the fracture of steel particles and spread on the magnesium side. With these results, it can be concluded that the stirring action of Tool II was more than other tools, and the stirring action of Tool IV was lower than in other cases. On the other hand, the average diameter of the particle of different joints revealed that the steel particles had 240, 220, 180, and 140 µm, respectively. These numbers indicate that the smaller particle fractured from the steel sheet with the increasing number of the shoulder.

The results indicated that the thickness of IMC at the interface of base metals is skinny. The high-magnification Sem image from the interface of Tool I, II and IV is presented in Fig. 9a–c, respectively. The results show that a

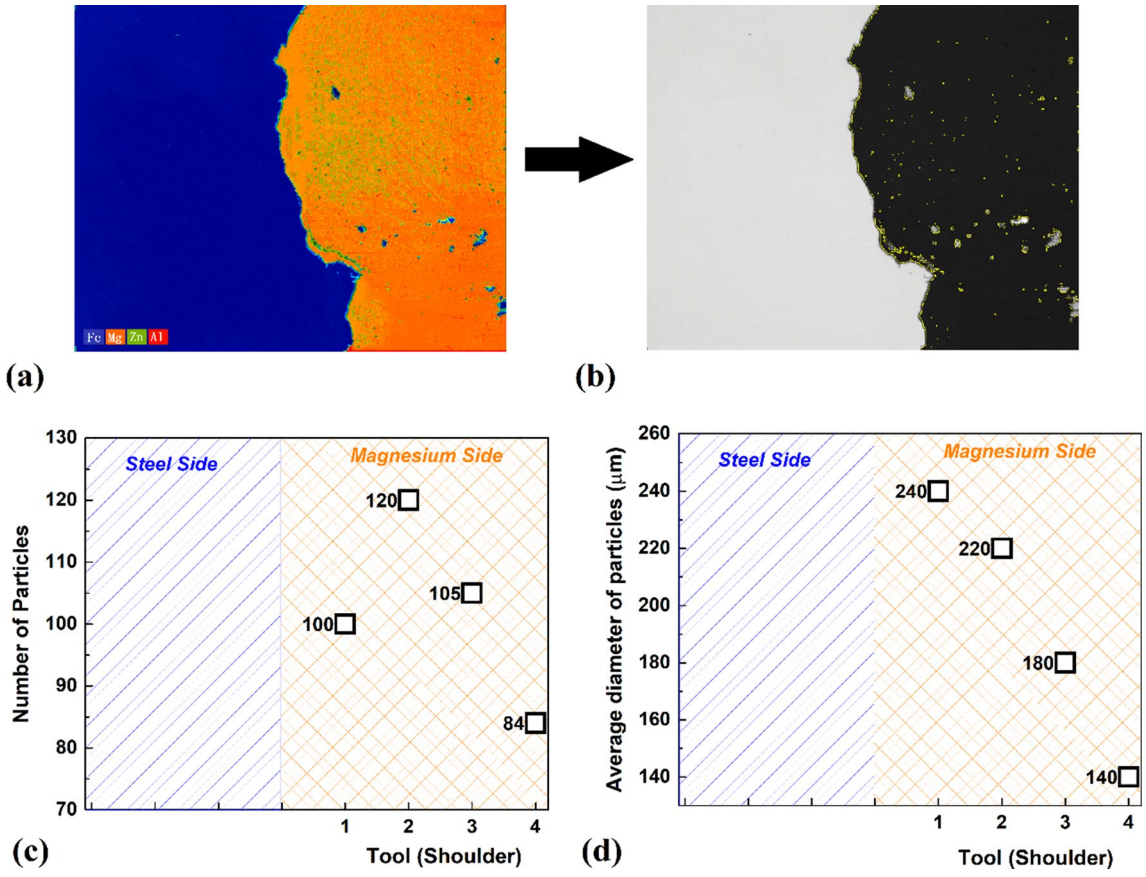

Fig. 8 **a** elements map from interface of joint that welded by Tool II, **b** image analysis of particle distribution in Tool II joint. The statistic results of **c** number of particles and **d** average diameter of particles that formed in SZ of joints with various number of tool shoulder

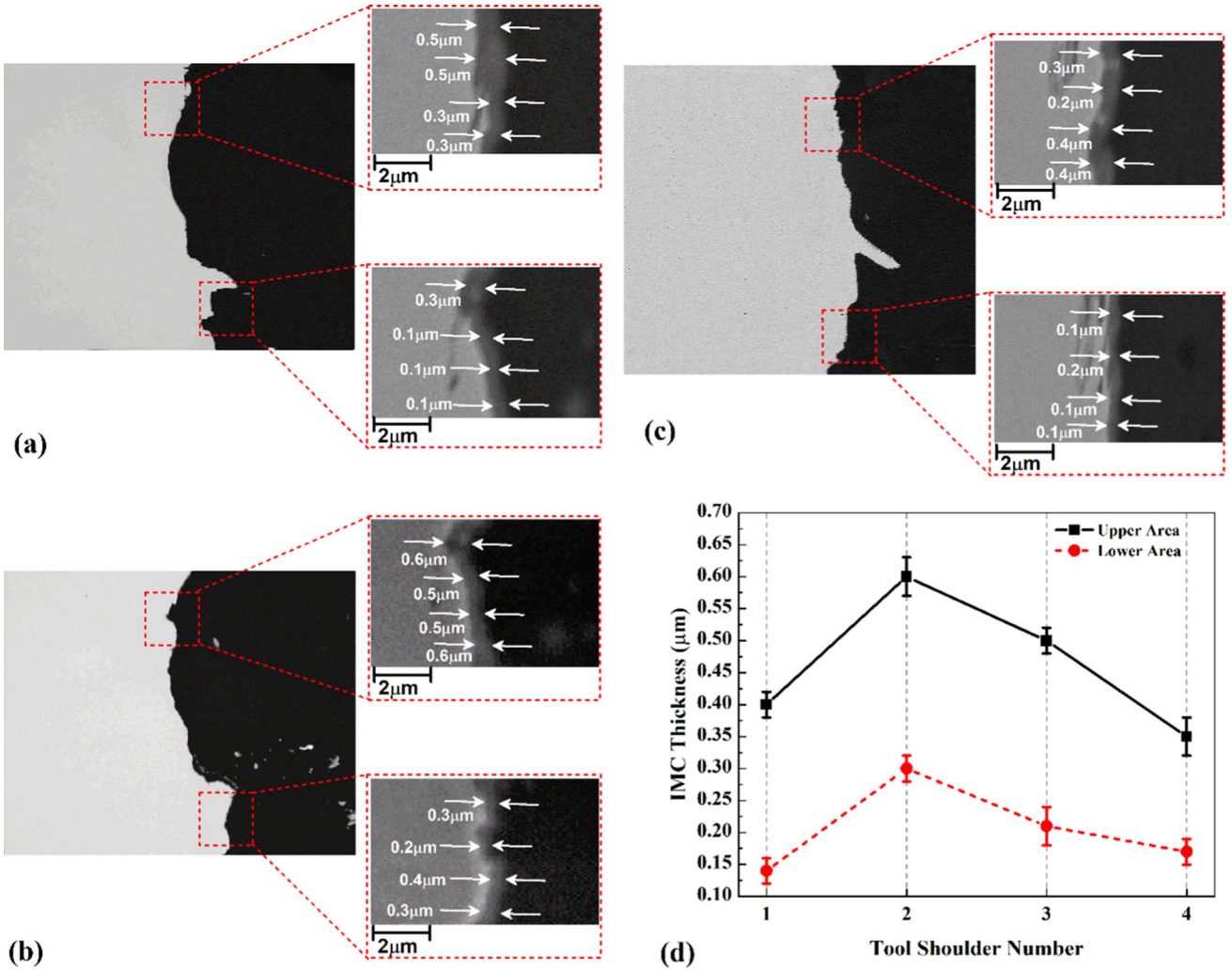

Fig. 9 High magnification SEM image from interface of joint that welded by **a** Tool I, **b** Tool II, **c** Tool IV and **d** thickness of IMC versus number of shoulders

narrow IMC layer was formed at the interface of base metals. As expected, due to the immiscibility of iron and magnesium elements, the thickness of IMC in this joint was very thin. This result indicates that the chemical bonding between AZ31 magnesium alloy and AISI 1006 steel was very low. The thickness of formed IMC at the upper and lower area of joints is presented in Fig. 9d. The results indicated that the average thickness of IMC at the upper area of joints welded using tools I, II, III, and IV was 0.4, 0.6, 0.52, and 0.53 μm, respectively. On the other hand, the average thickness of IMC at the lower area was 0.15, 0.3, 0.22 and 0.19 μm in the joint welded using tools I, II, III, and IV, respectively. It seems the amount of heat generation and stirring action of the tool is directly related to the thickness of IMC. As mentioned before, the Iron and Magnesium elements are immiscible, and the main result of the formation of IMC at the interface of welded samples is the presence of aluminium and zinc elements in the base metals composition. The line EDS results of the upper and lower area of the joint interface welded by Tool II are presented in Fig. 10a, b, respectively. The results indicated that the IMC layers are not uniform and, in some cases, are a mixture of various chemical compositions. As can be seen, in the upper area, the IMC was a combination of Mg_xZn_y and Fe_xAl. Due to obtained results, the exact composition of IMC predicted by the proportion of weight presents data obtained by EDS line scan. The results showed that Mg_4Zn_7 and Fe_2Al formed at the upper area of the interface. The Fe_2Al formed at the lower area of the interface. Due to obtained results, the higher stirring action and heat generation at the upper area lead to the formation of more complex IMC in the lower area of the stir zone. In this joint, the link between iron and magnesium atoms is made of aluminum atoms. In other words, aluminum elements greatly influence the chemical bonding between

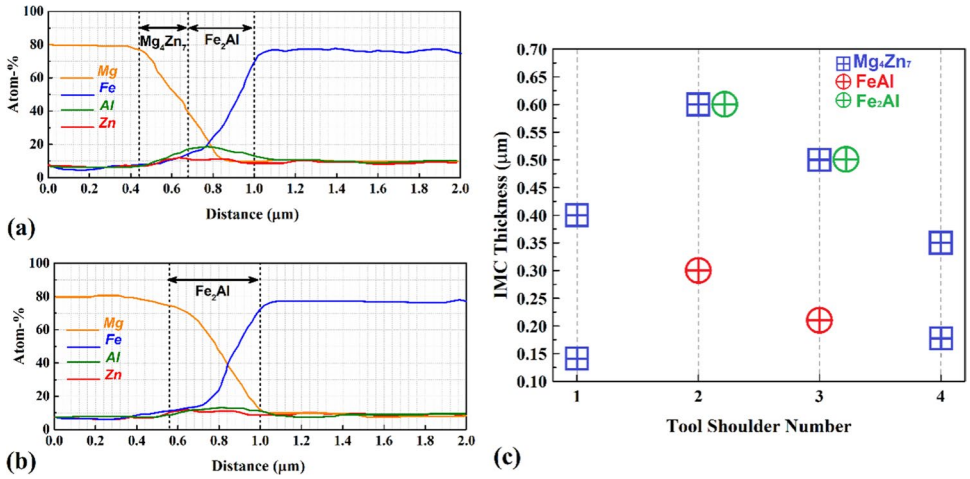

Fig. 10 EDS line scan from **a** upper and **b** lower area of joint that welded by Tool II. **c** IMC chemical composition versus number of shoulders

raw materials. Figure 10c presents the chemical composition of IMC at the interfaces of tools. The results indicated that the Mg_4Zn_7 and Fe_2Al were formed in Tool II and III joints. It seems the chemical composition of IMC in this joint is related to the thermo-mechanical action of tools. Higher thermo-machinal action leads to more complex and thicker IMC. The results revealed that the IMC composition at the upper area of joints welded using tools I and IV was Mg_4Zn_7. On the other hand, the lower area of the joint interface consists of different IMCs. The chemical composition of IMC at the lower area of Tool II and III was FeAl, and in Tool I and IV, they were mainly Mg_4Zn_7.

3.5 Tensile strength

As mentioned, three samples were extracted from each welded specimen to perform the tensile test. Figure 11a shows the changes in the studied samples' ultimate tensile stress (UTS). The reported UTS are obtained from the average of three tensile tests performed using tools I, II, III, and IV samples. According to the presented results, the UTS from high to low belongs to Tool II, III, I, and IV samples, respectively. The results indicate that the UTS of joints welded using tools I, II, III, and IV was 159, 208, 202, and 142 MPa, respectively. All samples were broken from the stir zone during the tensile test. It seems the quality of the mixture between raw metals at the stir zone determines the strength of the joints in this case. The tensile efficiency of the Tool II sample (as the highest UTS) is 77.6% compared to the softer alloy (AZ31 magnesium alloy). The tensile efficiency of the Tool IV sample (as the lowest UTS) is 52.9% compared to the AZ31 magnesium alloy. Based on the obtained results, it was found that the value of UTS of the welded samples is significantly dependent on the shoulder number.

According to the presented results, it was found that adding extra shoulders to the FSW tool significantly affects the strength of the welded samples. By comparing the UTS of samples, it was found that the most influential factor on the tensile strength of these samples is the mechanical interlock at the interface of base metals. Because the chemical bonding and IMC at the interface of AZ31 magnesium alloy and AISI 1006 steel is thin, the mechanical interlocks and wavy interface can improve the UTS. One or more than three shoulder tools are ineffective in increasing the mechanical interlock at the interface of base metals. Figure 11b–d show the SEM images of Tool I, II, and IV samples' fracture surfaces, respectively. In some areas of fracture surfaces, the lighter points that are steel fragments can be detected. The chemical bonding with Fe–Al–Mg described earlier caused those steel fragments to stack on the fracture surface. This steel fragments can play crack initiation during tensile test. Plus, small dimples can be detected on the fracture surface. In Tool II and IV, tensile test samples ripping fracture surfaces can be detected. The ripping fracture are fracture paths during tensile test. The more ripping fracture surface in Tool II revealed that the micro and macro scale mechanical interlocks, in this case, were more than other samples. It seems this type of fracture morphology is related to crack initiation from the wavy interface of welded samples. The results indicate that all sample fractures from the magnesium side of the stir zone. Due to low chemical interaction between base metals, the redundancy of steel base can be seen in the fracture surface. The fracture surface shows ductile fracture type with small dimples on the fracture surface.

3.6 Joint hardness

The hardness patterns of the welded samples are presented in this section. Figure 12 shows the hardness distribution of the welded samples by changing the number of shoulders of a pin. The results show that the HAZ has a lower hardness than raw materials on both sides. The hardness of TMAZ on the steel and magnesium sides was more than

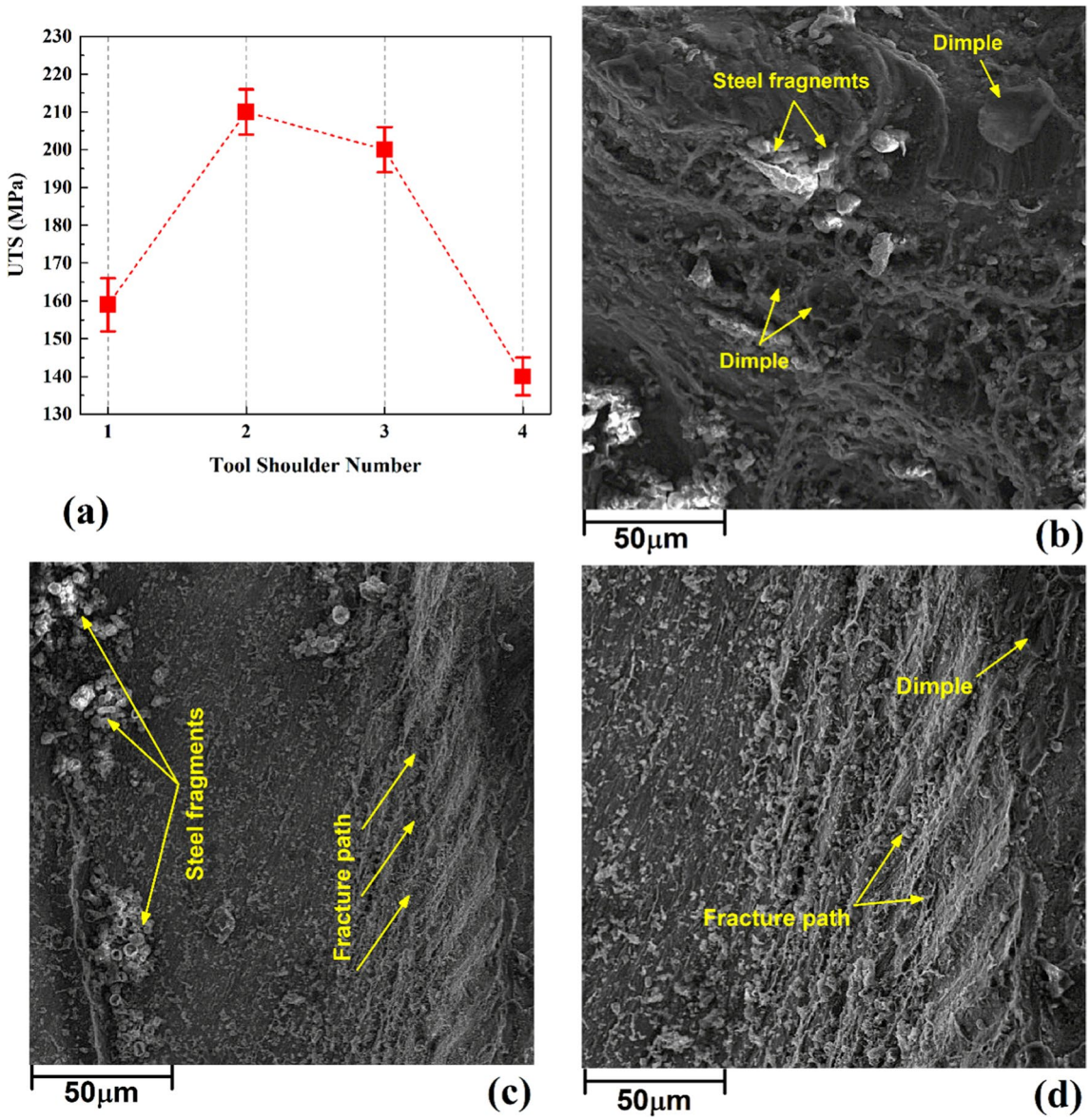

Fig. 11 **a** UTS versus tool shoulder number. The fracture surface of **b** Tool I, **c** Tool II and **d** Tool IV joints

HAZ and base metal hardness. This behavior can be seen in all samples. The results revealed that the hardness of the stir zone in all samples was more than the magnesium side. It seems the small steel particles that spread on the magnesium matrix increased the hardness of the stir zone. The results show that the stir zone of Tool II had the highest hardness, and tool IV had the lowest hardness. The average stir zone hardness of Tools I, II, III, and IV were recorded at 56 HB, 63 HB, 60 HB, and 58 HB, respectively. The tensile test revealed that the fracture location of the welded sample was on the magnesium side of the stir zone. Even though the average hardness of the stir zone was more than the HAZ and TMAZ areas of the magnesium side, the presence of steel fragments led to crack initiation and fracture of the FSWed joint from the stir zone area.

4 Conclusions

This research feasibility study on friction stir welding of AISI 1006 steel and AZ31 magnesium alloy has been investigated. Effects of tool shoulder number on material flow, joint formation, and mechanical properties analyzed, and the main results presented as:

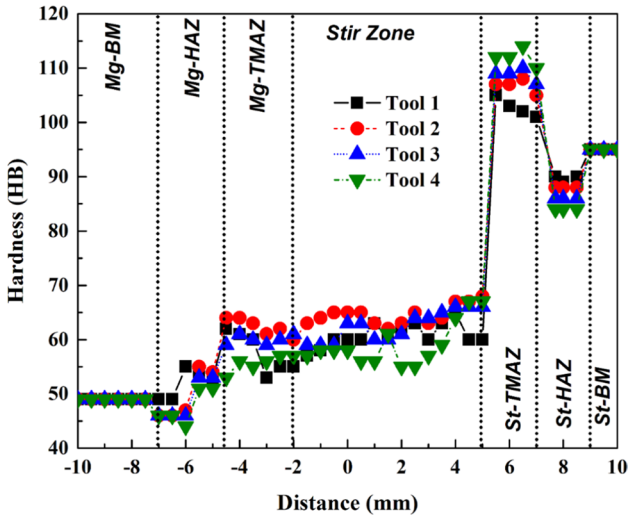

Fig. 12 hardness distribution along SZ of different joints.

1. The tool shoulder number has significant effects on internal material flow. The results indicated that the high number of shoulders has a negative effect on this joint, and a tool with more than three shoulders acts as a frustum pin during FSW. The tool with two shoulders shows a big difference in internal material flow compared to other tools.
2. The highest temperature recorded in the joint with Tool II at the steel side (603 °C) and the lowest temperature recorded in joint Tool IV at the magnesium side (400 °C). The surface flow of joints had no significant difference, and the microscale voids at the joint surface welded with Tool IV were maximum, and Tool II was minimum.
3. The chemical interaction between raw materials was not high, and a thin intermetallic compound formed at the interface of base materials due to the immiscibility of iron and magnesium elements. The presence of aluminium and zinc helped the formation of intermetallic compounds. The highest tensile strength was recorded for the joint welded by Tool II (208 MPa), and the main reason was increasing mechanical interlocks at the interface of base materials.

Author contributions RA: investigation, methodology, writing—original draft. HKH: investigation, data curation, writing—original draft. HAD: conceptualization, resources, supervision, writing—review and editing.

Data availability All data included in this study are available upon request by contact with the corresponding author.

Declarations

Conflict of interest The authors declare that there is no conflict of interest.

Ethical approval Not applicable.

Consent to participate Not applicable.

Consent for publication Not applicable.

References

1. Humpenöder F, et al. Land-use and carbon cycle responses to moderate climate change: Implications for land-based mitigation? Environ Sci Technol. 2015;49(11):6731–9. https://doi.org/10.1021/es506201r.
2. Kim HC, Wallington TJ. Life-cycle energy and greenhouse gas emission benefits of lightweighting in automobiles: review and harmonization. Environ Sci Technol. 2013;47(12):6089–97. https://doi.org/10.1021/es3042115.
3. Patel M, Pardhi B, Chopara S, Pal M. Lightweight composite materials for automotive—a review. Concepts J Appl Res. 2018;3(7):41–7.
4. Jiang H, Liao Y, Gao S, Li G, Cui J. Comparative study on joining quality of electromagnetic driven self-piecing riveting, adhesive and hybrid joints for Al/steel structure. Thin-Walled Struct. 2021;164:107903. https://doi.org/10.1016/J.TWS.2021.107903.
5. Jiang H, Liao Y, Jing L, Gao S, Li G, Cui J. Mechanical properties and corrosion behavior of galvanized steel/Al dissimilar joints. Archiv Civil Mech Eng. 2021. https://doi.org/10.1007/s43452-021-00320-5.
6. Chen YC, Nakata K. Friction stir lap welding of magnesium alloy and zinc-coated steel. Mater Trans. 2009;50(11):2598–603. https://doi.org/10.2320/matertrans.M2009022.
7. Al-Sabur R. Tensile strength prediction of aluminium alloys welded by FSW using response surface methodology—comparative review. Mater Today Proc. 2021. https://doi.org/10.1016/j.matpr.2020.12.1001.
8. Chikh A, Serier M, Al-Sabur R, Siddiquee AN, Gangil N. Thermal modeling of tool-work interface during friction stir welding process. Russ J Non-Ferrous Met. 2022;63(6):690–700. https://doi.org/10.3103/S1067821222060049.
9. Ghiasvand A, Noori SM, Suksatan W, Tomków J, Memon S, Derazkola HA. Effect of tool positioning factors on the strength of dissimilar friction stir welded joints of AA7075-T6 and AA6061-T6. Materials. 2022;15(7):2463. https://doi.org/10.3390/ma15072463.
10. Al-Sabur RK, Jassim AK. Friction stir spot welding applied to weld dissimilar metals of AA1100 Al-alloy and C11000 copper. IOP Conf Ser Mater Sci Eng. 2018. https://doi.org/10.1088/1757-899X/455/1/012087.
11. Memon S, Tomków J, Derazkola HA. Thermo-mechanical simulation of underwater friction stir welding of low carbon steel. Materials. 2021;14(17):4953. https://doi.org/10.3390/ma14174953.
12. Khalaf HI, Al-sabur R, Abdullah ME, Kubit A, Derazkola HA. Effects of underwater friction stir welding heat generation on residual stress of AA6068-T6 aluminum alloy. Materials. 2022;15(6):2223. https://doi.org/10.3390/ma15062223.
13. Al-Sabur R, Khalaf HI, Świerczyńska A, Rogalski G, Derazkola HA. Effects of noncontact shoulder tool velocities on friction stir joining of polyamide 6 (PA6). Materials. 2022;15(12):4214.

14. Derazkola HA, Simchi A. An investigation on the dissimilar friction stir welding of T-joints between AA5754 aluminum alloy and poly(methyl methacrylate). Thin-Walled Struct. 2019;135:376–84. https://doi.org/10.1016/j.tws.2018.11.027.
15. Abe Y, Watanabe T, Tanabe H, Kagiya K. Dissimilar metal joining of magnesium alloy to steel by FSW. Adv Mater Res. 2007;15–17:393–7. https://doi.org/10.4028/www.scientific.net/amr.15-17.393.
16. Watanabe T, Kagiya K, Yanagisawa A, Tanabe H. Solid state welding of steel and magnesium alloy using a rotating pin—Solid state welding of dissimilar metals using a rotating pin (report 3). Yosetsu Gakkai Ronbunshu/Q J Jpn Weld Soc. 2006;24(1):108–15. https://doi.org/10.2207/qjjws.24.108.
17. Jana S, Hovanski Y, Grant GJ. Friction stir lap welding of magnesium alloy to steel: a preliminary investigation. Metall Mater Trans A Phys Metall Mater Sci. 2010;41(12):3173–82. https://doi.org/10.1007/s11661-010-0399-8.
18. Schneider C, Weinberger T, Inoue J, Koseki T, Enzinger N. Characterization of interface of steel/magnesium FSW. Sci Technol Weld Join. 2011;16(1):100–7. https://doi.org/10.1179/136217810Y.0000000012.
19. Jana S, Hovanski Y. Fatigue behaviour of magnesium to steel dissimilar friction stir lap joints. Sci Technol Weld Join. 2012;17(2):141–5. https://doi.org/10.1179/1362171811Y.0000000083.
20. Chen YC, Nakata K. Effect of tool geometry on microstructure and mechanical properties of friction stir lap welded magnesium alloy and steel. Mater Des. 2009;30(9):3913–9. https://doi.org/10.1016/j.matdes.2009.03.007.
21. Zhang ZK, Wang XJ, Wang PC, Zhao G. Friction stir key holeless spot welding of AZ31 Mg alloy-mild steel. Trans Nonferrous Met Soc China (English Edn). 2014;24(6):1709–16. https://doi.org/10.1016/S1003-6326(14)63244-1.
22. Wei Y, Li J, Xiong J, Huang F, Zhang F. Microstructures and mechanical properties of magnesium alloy and stainless steel weld-joint made by friction stir lap welding. Mater Des. 2012;33(1):111–4. https://doi.org/10.1016/j.matdes.2011.07.016.
23. Uematsu Y, Kakiuchi T, Tozaki Y, Kojin H. Comparative study of fatigue behaviour in dissimilar Al alloy/steel and Mg alloy/steel friction stir spot welds fabricated by scroll grooved tool without probe. Sci Technol Weld Join. 2012;17(5):348–56. https://doi.org/10.1179/1362171812Y.0000000014.
24. Kulkarni SS, et al. A combined experimental and modeling approach to investigate the performance of joint between AZ31 magnesium and uncoated DP590 steel using friction stir-assisted scribe technique. J Mater Eng Perform. 2021;30(11):8293–308. https://doi.org/10.1007/s11665-021-06060-0.
25. Das H, Upadhyay P, Wang T, Gwalani B, Ma X. Interfacial reaction during friction stir assisted scribe welding of immiscible Fe and Mg alloy system. Sci Rep. 2021. https://doi.org/10.1038/s41598-021-81266-9.
26. Sahu S, Mypati O, Pal SK, Shome M, Srirangam P. Effect of weld parameters on joint quality in friction stir welding of Mg alloy to DP steel dissimilar materials. CIRP J Manuf Sci Technol. 2021;35:502–16. https://doi.org/10.1016/j.cirpj.2021.06.012.
27. Fu B, et al. Revealing joining mechanism in refill friction stir spot welding of AZ31 magnesium alloy to galvanized DP600 steel. Mater Des. 2021;209:109997. https://doi.org/10.1016/j.matdes.2021.109997.
28. Chen Y, Chen J, ShalchiAmirkhiz B, Worswick MJ, Gerlich AP. Microstructures and properties of Mg alloy/DP600 steel dissimilar refill friction stir spot welds. Sci Technol Weld Join. 2015;20(6):494–501. https://doi.org/10.1179/1362171815Y.0000000033.
29. Shen Z, Ding Y, Chen J, Gerlich AP. Comparison of fatigue behavior in Mg/Mg similar and Mg/steel dissimilar refill friction stir spot welds. Int J Fatigue. 2016;92:78–86. https://doi.org/10.1016/j.ijfatigue.2016.06.033.
30. Liyanage T, Kilbourne J, Gerlich AP, North TH. Joint formation in dissimilar Al alloy/steel and Mg alloy/steel friction stir spot welds. Sci Technol Weld Join. 2009;14(6):500–8. https://doi.org/10.1179/136217109X456960.
31. Singh VP, Patel SK, Kumar N, Kuriachen B. Parametric effect on dissimilar friction stir welded steel–magnesium alloys joints: a review. Sci Technol Weld Join. 2019;24(8):653–84. https://doi.org/10.1080/13621718.2019.1567031.
32. Zhang YN, Cao X, Larose S, Wanjara P. Review of tools for friction stir welding and processing. Can Metallur Q. 2012;51(3):250–61. https://doi.org/10.1179/1879139512Y.0000000015.